Supplement of Atmos. Chem. Phys., 25, 13995–14013, 2025 https://doi.org/10.5194/acp-25-13995-2025-supplement © Author(s) 2025. CC BY 4.0 License.





Supplement of

Prior heterogeneous ice nucleation events shape homogeneous freezing during the evolution of synoptic cirrus

Kasper Juurikkala et al.

Correspondence to: Kasper Juurikkala (kasper.juurikkala@fmi.fi)

The copyright of individual parts of the supplement might differ from the article licence.

S1 Sensitivity of wind fluctuations to changes in domain width and grid resolution

A sensitivity test was conducted to look into the sensitivity of the wind fluctuations by changing the horizontal domain horizontal width from 3 km to 6 km. Also, a simulation run with lower resolution Δx = 150 m and 18 x 18 km domain was conducted. Figure S1 shows vertical wind at approximately 11 km altitude. The 18 km domain resolved large wavelengths while there was a lack of shorter wavelengths resolved. The 6 km domain resolved longer wavelengths as well as shorter wavelengths. This is due to the higher resolution of Δx = 50 m. The 3 km model domain resolved only small scale waves. Also, the horizontal variability of temperature and humidity did not differ significantly. In contrast, the 18 km domain had no significant horizontal variations in temperature and humidity due to unresolved small scale waves. Based on these results, the 3D simulations were conducted using a 3 km domain, as it provided wind variability comparable to that of larger domains while significantly minimizing computational costs.

On the other hand, the bottom right plot in Figure S1 shows the vertical wind when the ice nucleation scheme was turned off. It is clear that the ice nucleation had no major correlation with the vertical wind fluctuations.

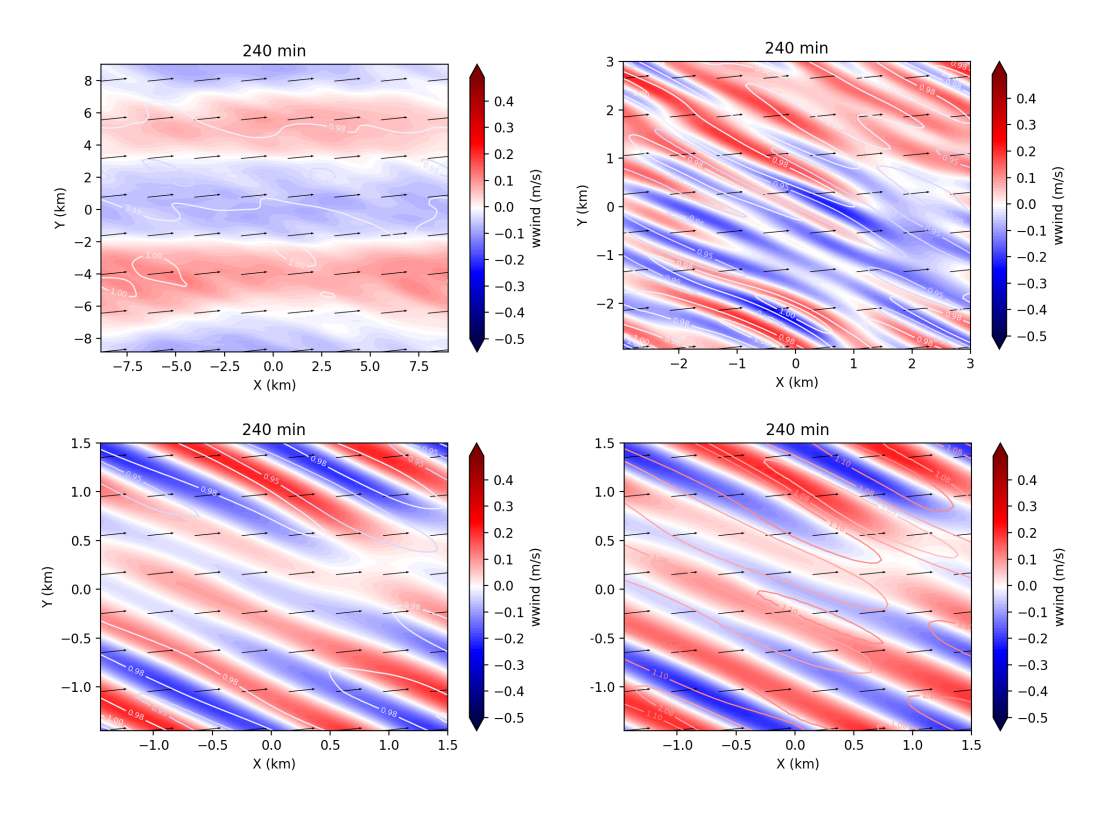


Figure S1. Vertical wind in 18 km (upper left), 6 km (upper right) and 3 km domain (lower left) at 3 hours into the simulation on 11 km altitude. Lower right plot shows the case without ice nucleation. S_i is indicated with colored contours. The vectors represent the horizontal wind direction and magnitude.

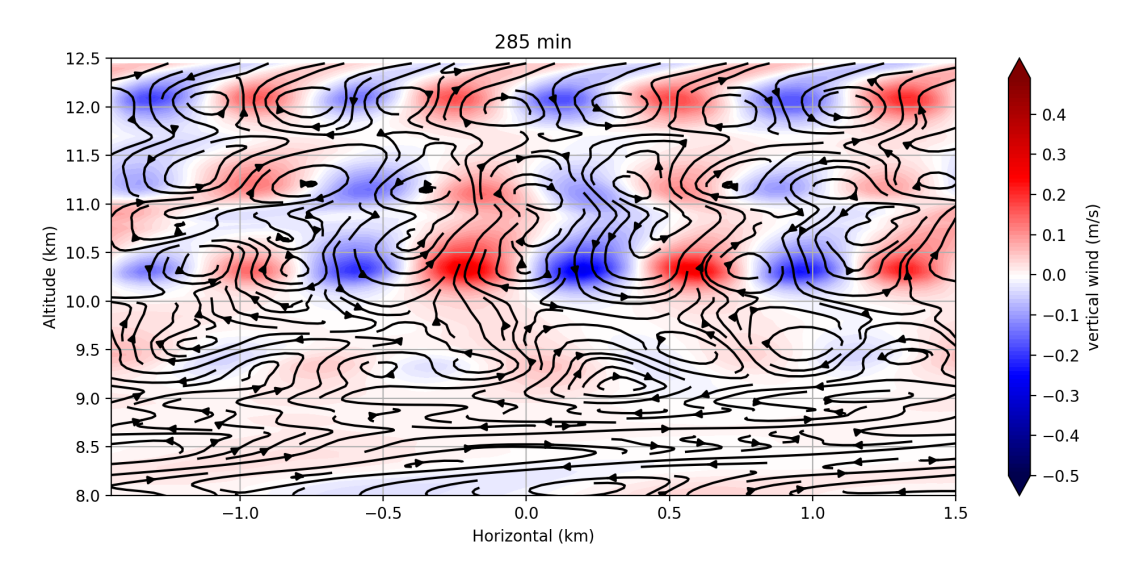


Figure S2. Gravity waves induced by vertical wind shear. Horizontal eddies shown with streamlines on y-axis plane.

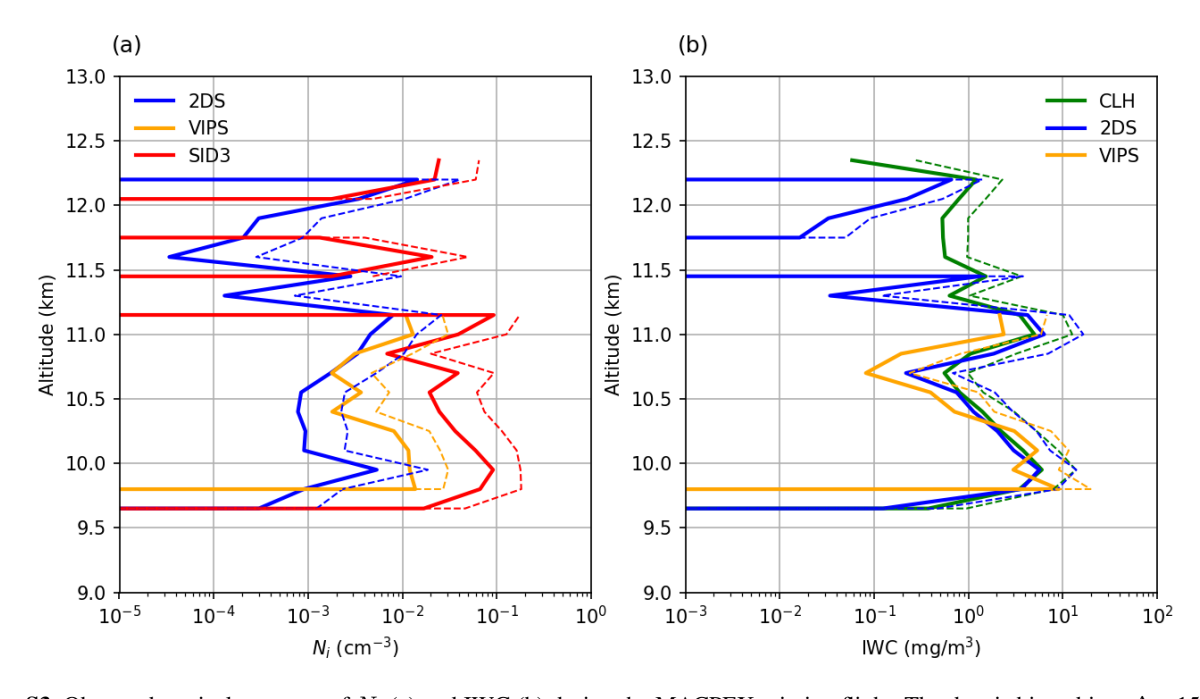


Figure S3. Observed vertical structure of N_i (a) and IWC (b) during the MACPEX mission flight. The data is binned into Δz =150 m wide bins. The dashed lines represent 1-sigma standard deviation of a bin.

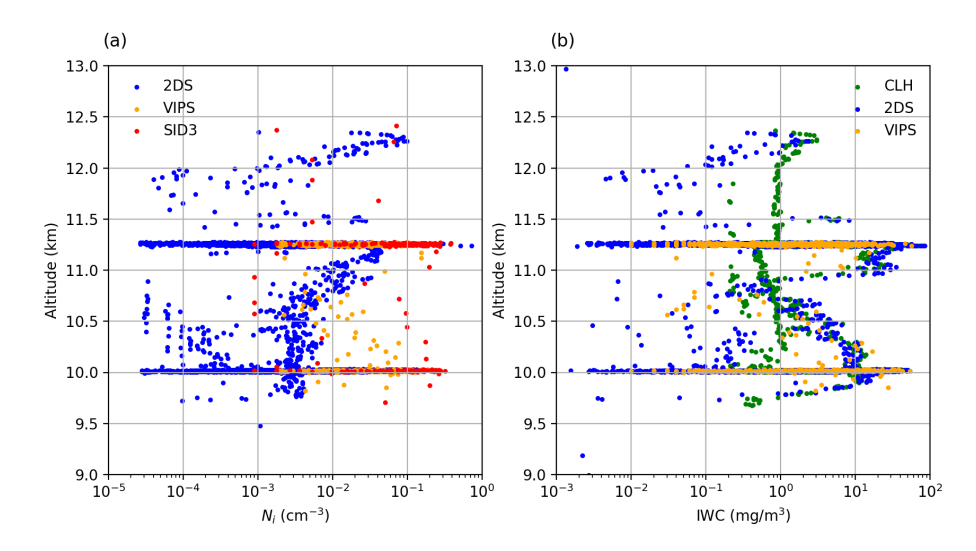


Figure S4. Observed vertical structure of N_i (a) and IWC (b) during the MACPEX mission flight.

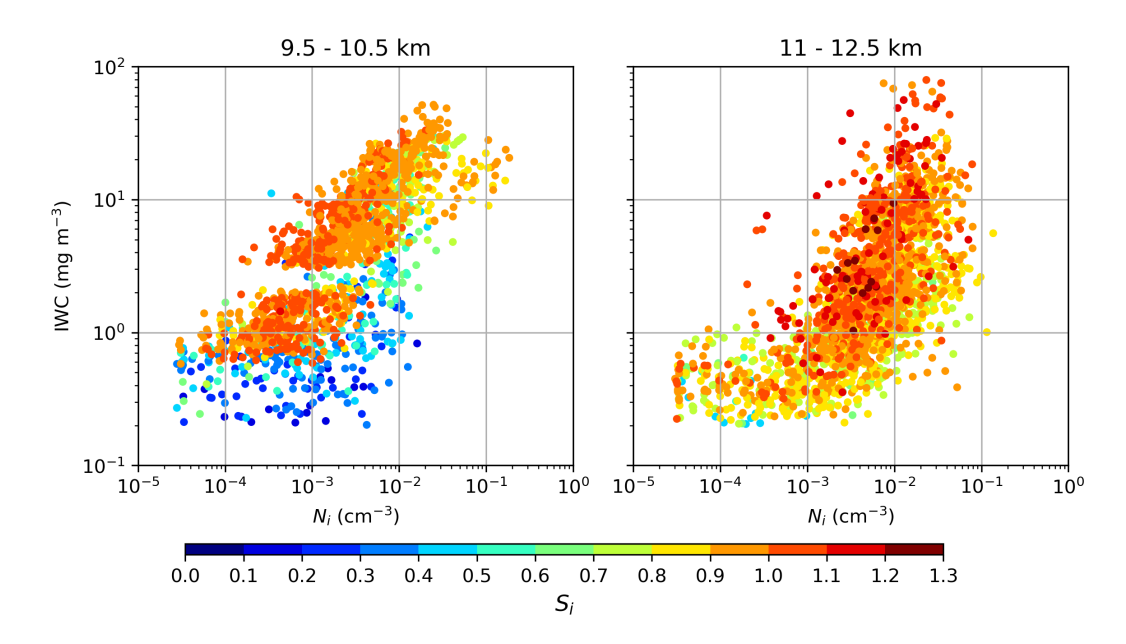


Figure S5. 1:1 scatter plot of N_i (x-axis, 2DS) and IWC (y-axis, CLH). Coloring shows S_i binned in 0.1 interval.

S3 Description of ice nucleation parameterization scheme by Ullrich et al. (2017)

15 Ullrich et al. (2017) parameterization scheme for deposition ice nucleation, is based on 11 years worth of laboratory experiments conducted in the Aerosol Interaction and Dynamics in the Atmosphere (AIDA) chamber. This framework was specifically developed to assess the nucleation characteristics of mineral dust and soot particles under conditions relevant to cirrus clouds (Ullrich et al., 2019). The parameterization presented below quantifies the nucleation ability of mineral dust/soot particles in terms of ice nucleation active site (INAS) density n_s (e.g., Hoose and Möhler, 2012; Vali et al., 2015). The INAS density represents the number of active sites per unit surface area of an INP (m⁻²) at a specific temperature and S_i. These active sites are locations on the particle surface where nucleation occurs more effectively, typically resulting from surface inhomogeneities (Vali et al., 2015). The parametrization is given by:

$$n_s = \exp\{\alpha(S_i - 1)^{1/4}\cos[\beta(T - \gamma)]^2 \operatorname{arccot}[\kappa(T - \lambda)]/\pi\}$$

$$\operatorname{arccot}(\mathbf{x}) = \frac{\pi}{2} - \arctan(\mathbf{x})$$
(S1)

25 where the parameters and corresponding values for mineral dust are given in Table S1.

	α	β	γ	κ	λ	Valid temperature range (K)
Mineral dust	285.692	0.017	256.692	0.080	200.745	[206, 240]

Table S1. Fit parameters for equation 2.11 for mineral dust particles. The parametrization is valid for S_i below water saturation, homogeneous nucleation threshold and above 1.0.

Predicted frozen fraction FF of INPs can be calculated by multiplying the INAS density by the surface area of INPs with a single particle size.

$$FF = n_s S_X = n_s \pi D_X^2 \tag{S2}$$

S4 Homogeneous freezing parametrization by Koop et al. (2000)

The parametrization for homogeneous freezing follows Koop et al. (2000) formulation. The nucleation rate is parametrized with shift in melting curve $\Delta a_w = a_w - a_w^i$. In Koop (2015), the $a_w^i = \frac{p_{\text{ice}}(T)}{p_{\text{liq}}(T)}$. Knowing this an equation follows:

$$\Delta a_w = a_w - a_w^i = \frac{p_v}{p_{\text{liq}}(T)} - \frac{p_{\text{ice}}(T)}{p_{\text{liq}}(T)}$$
(S3)

Koop et al. (2000) parametrizations produces freezing rate $(cm^{-3}s^{-1})$ as:

35

$$\log(J) = -906.7 + 8502\Delta a_w - 26924(\Delta a_w)^2 + 29180(\Delta a_w)^3$$
(S4)

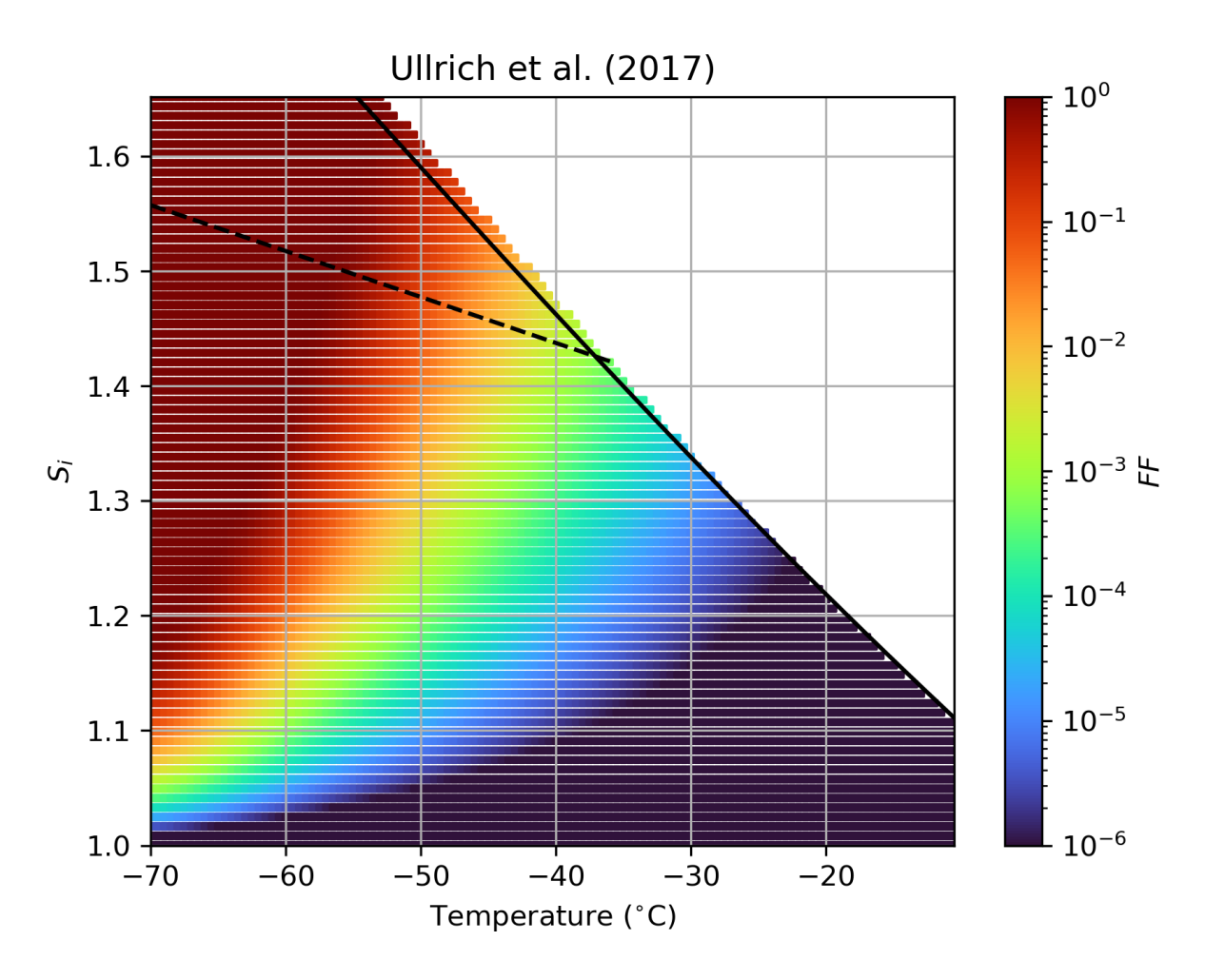


Figure S6. Frozen fraction of mineral dust particles used in this study. The activity is integrated over the mineral dust particle sizes to reflect the total activity. Dashed line indicates Koop et al. (2000) line at the critical threshold for homogeneous freezing. Solid line follows water saturation (Murphy and Koop, 2005).

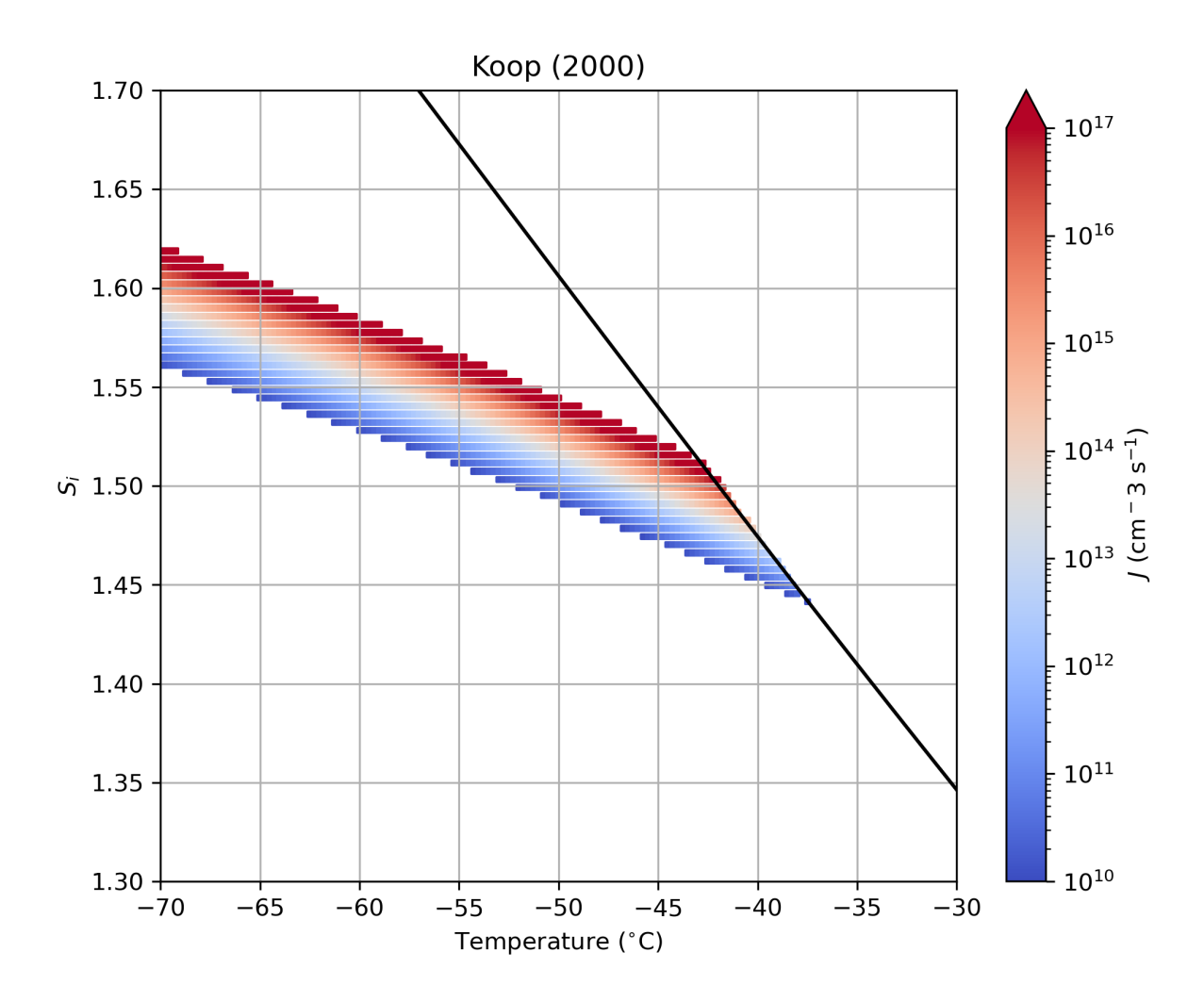


Figure S7. Koop et al. (2000) parametrization scheme as a function of temperature and Δa_w . Solid line indicates the water saturation line.

S5 Additional model settings

Once ice nucleation occurs in SALSA, ice crystals grow via a vapour deposition scheme according to formulation by Jacobson (2005). The ice crystal bins represent ice crystal mass sizes ranging from 2 to 500 μ m. For processes such as sedimentation, condensation, and coagulation, only ice-related particle processes are modelled, with an exception on condensation of water vapour on aerosol particles to enable homogeneous freezing. Ice crystals are assumed to be spherical for sizes below 40 μ m and bullet rosettes for larger particles. The habit dependence on size roughly follows the suggestion by Baum et al. (2005), which indicates that ice crystals below 60 μ m are droxtals, while larger particles exhibit more complex habits. Images captured with the 2DS instrument during the April 16th flight show that a significant portion of larger ice crystals were bullet rosettes. To include the habit dependence on the crystal size, modification to mass transfer parametrizations were made. The capacitance was modified to reflect the increase in complexity of the ice crystal habit for larger crystals:

$$C_i(D_i) = \begin{cases} 0.5D_i, D_i < 40 \,\mu\text{m} \\ 0.25D_i, D_i \ge 40 \,\mu\text{m} \end{cases}$$

, where D_i is the diameter maximum size of an ice crystal. Additionally, the ice crystal shape parameters (mass-diameter and area-diameter relationship parameters) were modified to accommodate the habit dependency by crystal size and are given in Table S2. SALSA calculates terminal velocity of ice crystals by the formulation described in Mitchell and Heymsfield (2005) (previous versions of SALSA use the Khvorostyanov and Curry (2002) formulation).

	α	β	γ	σ	
Spherical	$\frac{\pi}{6}\rho_p$	3	$\frac{\pi}{4}$	2	D_i < 40 μ m
Bullet rosette (5-sided)	0.0138	2.26	0.2148	1.7956	$D_i > 40 \ \mu \text{m}$

Table S2. Values for parameters in mass-diameter and area-diameter relationships. The relationship between mass and diameter is given as $m = \alpha D_i^{\beta}$. The projected area and diameter relationship is given as $A = \gamma D_i^{\sigma}$.

In addition, the existing vapor mass flux equation inside SALSA was modified to include the mass accommodation coefficient for water vapor uptake of ice crystals (α_c) and it is set at $\alpha_c=0.5$ for this case study. This value has a large uncertainty currently with measurements showing values in range $0.004 \ge \alpha_c \ge 1.06$ (see, Skrotzki et al., 2013). By default the α_c was practically set at 1 previously (with no parameter described), however, this value falls in the high end of the typically observed values.

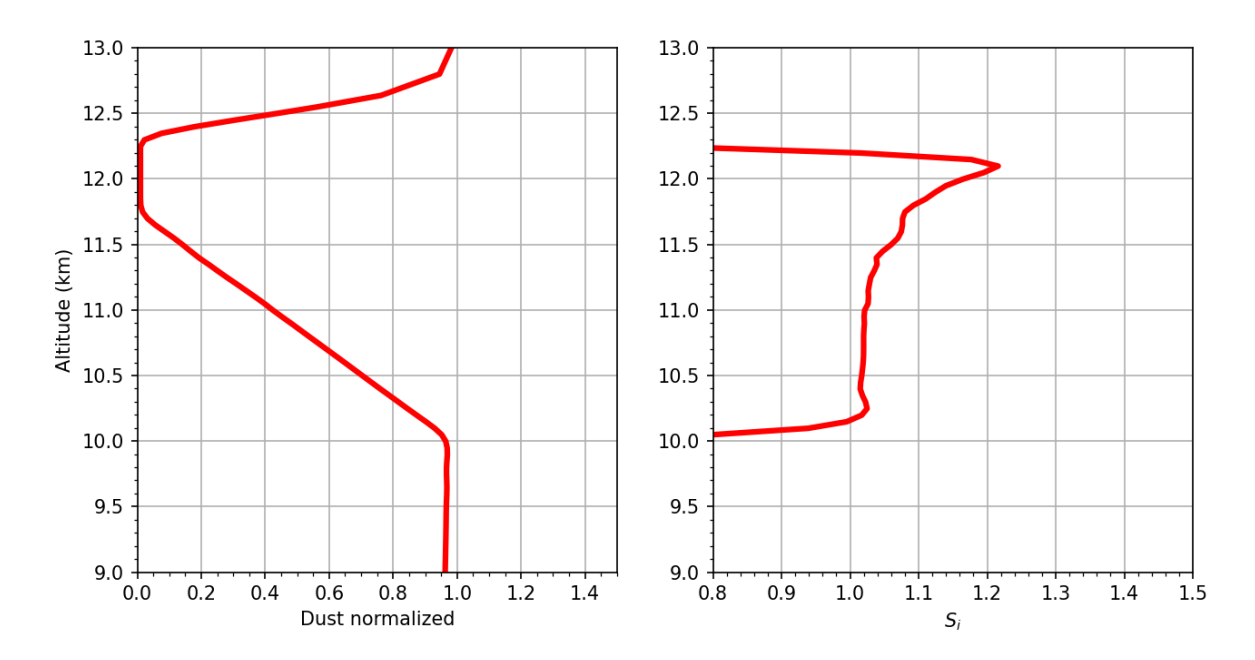


Figure S8. Initial profile of dust and S_i for adjusted profile runs.

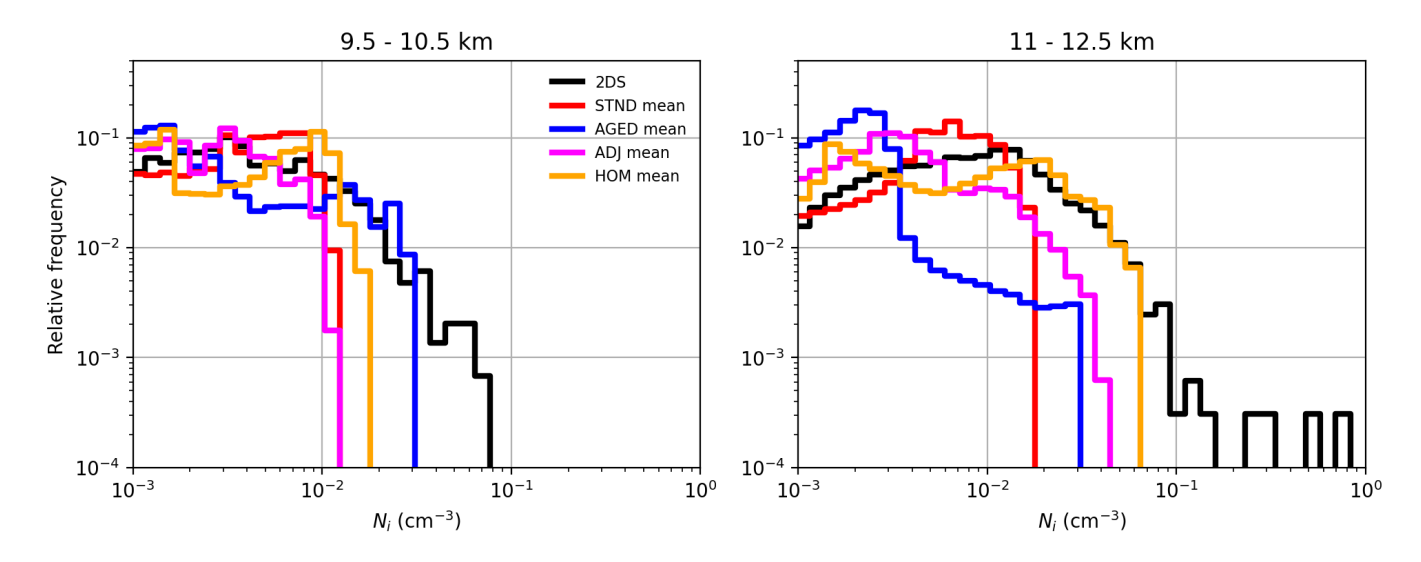


Figure S9. Frequency distributions for all setups in the study with 1D-column setup.

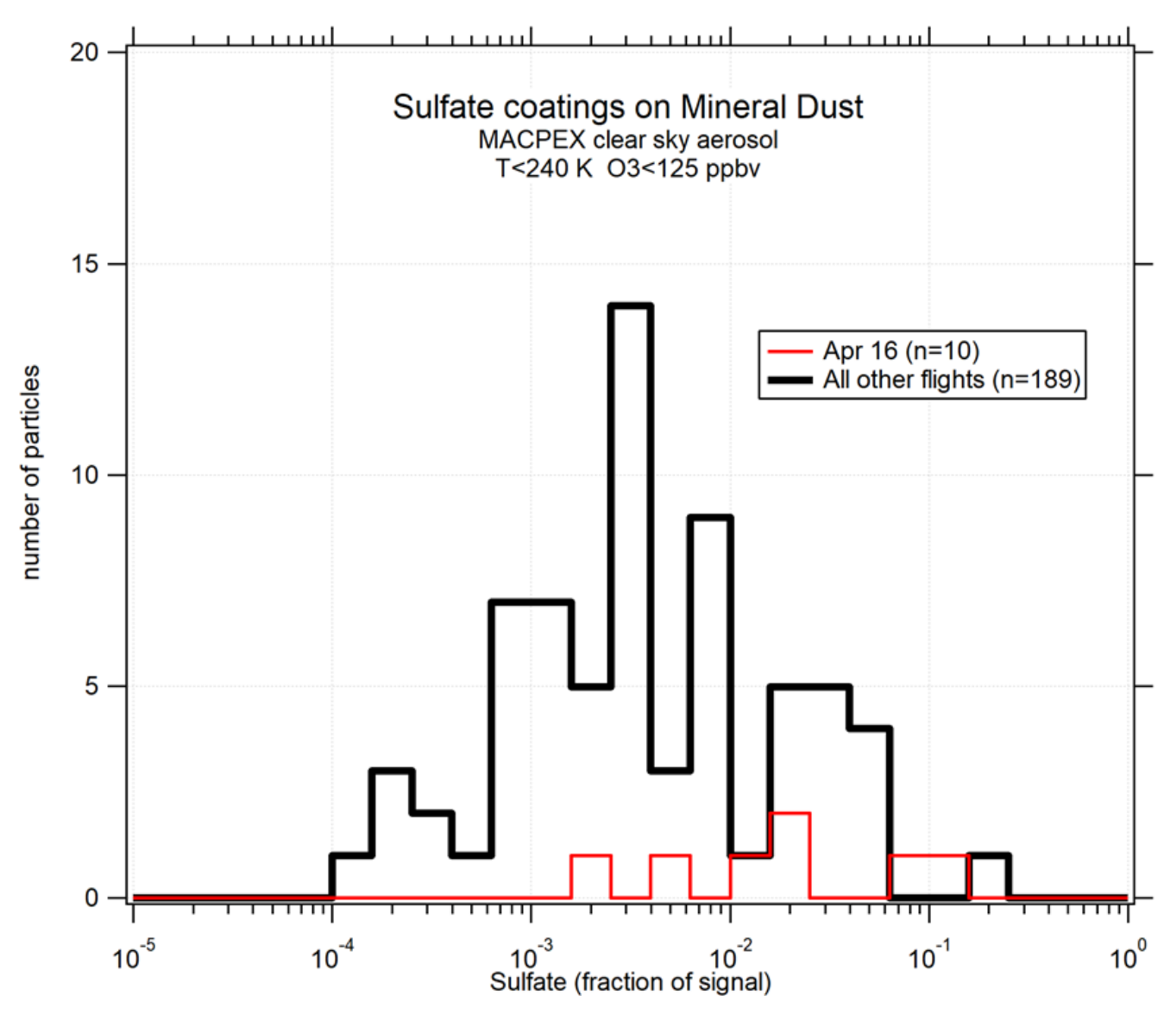


Figure S10. The raw sulfate signal on all clear-sky mineral dust spectra, comparing Apr 16 cirrus regime with all other flight days. The statistics are poor, but this "is consistent with" the idea that well-aged UT air gives rise to thicker coatings on dust particles that could potentially reduce their heterogeneous nucleation ability.

References

70

85

- Baum, B. A., Heymsfield, A. J., Yang, P., and Bedka, S. T.: Bulk Scattering Properties for the Remote Sensing of Ice Clouds. Part I: Microphysical Data and Models, Journal of Applied Meteorology, 44, 1885 1895, https://doi.org/10.1175/JAM2308.1, 2005.
 - Hoose, C. and Möhler, O.: Heterogeneous ice nucleation on atmospheric aerosols: a review of results from laboratory experiments, Atmospheric Chemistry and Physics, 12, 9817–9854, https://doi.org/10.5194/acp-12-9817-2012, 2012.
 - Jacobson, M. Z.: Fundamentals of Atmospheric Modeling, Cambridge University Press, 2 edn., 2005.
- 65 Khvorostyanov, V. I. and Curry, J. A.: Terminal Velocities of Droplets and Crystals: Power Laws with Continuous Parameters over the Size Spectrum, Journal of the Atmospheric Sciences, 59, 1872 1884, https://doi.org/10.1175/1520-0469(2002)059<1872:TVODAC>2.0.CO;2, 2002.
 - Koop, T.: Atmospheric Water, in: Water: Fundamentals as the Basis for Understanding the Environment and Promoting Technology, edited by: Debenedetti, P. G., Ricci, A., and Bruni, F., IOS, Amsterdam, Bologna, https://doi.org/https://doi.org/10.3254/978-1-61499-507-4-45, 2015.
 - Koop, T., Luo, B., Tsias, A., and Peter, T.: Water Activity as the determinant for homogeneous ice nucleation in aqueous solutions, Nature, 406, 611–4, https://doi.org/10.1038/35020537, 2000.
 - Mitchell, D. L. and Heymsfield, A. J.: Refinements in the Treatment of Ice Particle Terminal Velocities, Highlighting Aggregates, Journal of the Atmospheric Sciences, 62, 1637 1644, https://doi.org/10.1175/JAS3413.1, 2005.
- Murphy, D. M. and Koop, T.: Review of the vapour pressures of ice and supercooled water for atmospheric applications, Quarterly Journal of the Royal Meteorological Society, 131, 2005.
 - Skrotzki, J., Connolly, P., Schnaiter, M., Saathoff, H., Möhler, O., Wagner, R., Niemand, M., Ebert, V., and Leisner, T.: The accommodation coefficient of water molecules on ice cirrus cloud studies at the AIDA simulation chamber, Atmospheric Chemistry and Physics, 13, 4451–4466, https://doi.org/10.5194/acp-13-4451-2013, 2013.
- 80 Ullrich, R., Hoose, C., Möhler, O., Niemand, M., Wagner, R., Höhler, K., Hiranuma, N., Saathoff, H., and Leisner, T.: A New Ice Nucleation Active Site Parameterization for Desert Dust and Soot, Journal of the Atmospheric Sciences, 74, 699 717, https://doi.org/10.1175/JAS-D-16-0074.1, 2017.
 - Ullrich, R., Hoose, C., Cziczo, D. J., Froyd, K. D., Schwarz, J. P., Perring, A. E., Bui, T. V., Schmitt, C. G., Vogel, B., Rieger, D., Leisner, T., and Möhler, O.: Comparison of Modeled and Measured Ice Nucleating Particle Composition in a Cirrus Cloud, Journal of the Atmospheric Sciences, 76, 1015 1029, https://doi.org/10.1175/JAS-D-18-0034.1, 2019.
 - Vali, G., DeMott, P. J., Möhler, O., and Whale, T. F.: Technical Note: A proposal for ice nucleation terminology, Atmospheric Chemistry and Physics, 15, 10 263–10 270, https://doi.org/10.5194/acp-15-10263-2015, 2015.